STRUCTURAL CONTROL AND HEALTH MONITORING
*Struct. Control Health Monit.* 2015; **22**:314–329
Published online 13 June 2014 in Wiley Online Library (wileyonlinelibrary.com). DOI: 10.1002/stc.1675

# Localization of acoustic emission sources in structural health monitoring of masonry bridge

Qinghua Han[1], Jie Xu[1,*,†], Alberto Carpinteri[2] and Giuseppe Lacidogna[2]

[1]*School of Civil Engineering/Key Laboratory of Coast Civil Structure Safety, Ministry of Education, Tianjin University, Tianjin 300072, China*
[2]*Department of Structural, Geotechnical and Building Construction, Politecnico di Torino, Torino, Italy*

SUMMARY

The application of the acoustic emission (AE) technique to monitoring the crack characterization in masonry structures is investigated in this paper. An improved approach, modified from the classical crack source localization method, is proposed to provide more reliable crack locations in masonry structures. The introduced parameter, degree of inhomogeneity $\xi$ in the modified method, can help to decrease the unavoidable propagation delay related to refraction due to the layers in masonry material. The modified method is successfully applied to the AE source detection during the pencil-lead break test and the central pier settlement test of a masonry model bridge to analyze the crack pattern. It is shown that the proposed method is a reliable tool for crack source location in masonry structures. Copyright © 2014 John Wiley & Sons, Ltd.

Received 9 August 2013; Revised 14 May 2014; Accepted 24 May 2014

KEY WORDS: acoustic emission; source localization method; masonry bridge; propagation delay; degree of inhomogeneity

## 1. INTRODUCTION

Various masonry structures, such as towers, bridges, and historical buildings are widely distributed all over the world. As a consequence of building with old techniques, long-time exposing to the environmental conditions and changing loading regimes, many of these masonry structures are placed in repair and strengthening programs [1,2]. Prior to repair and rehabilitation, inspections of the structures to estimate the current state in service are essentially required. Therefore, it is imperative that sound safety assessment methods are available in order to preserve these inestimable cultural heritages. As one of the non-destructive evaluation and diagnostic techniques, acoustic emission (AE) technique can be employed in the masonry monitoring [3–7].

Within civil engineering practice, the AE technique is a promising non-destructive technique for the detection of damage onset and growth [8–10]. AE is the class of phenomena whereby transient elastic waves are generated by the rapid release of strain energy when damage occurs within a material. By investigating acoustic signals' onset times and other characteristics, AE techniques provide an insight into the deterioration processes of a tested object [11,12]. As the onset times of AE signals at different sensors are linked to the propagation speed inside the material, algorithms can be used to locate the emitting sources and to predict their subsequent development [1,7]. AE is already widely used for monitoring metallic [13,14], rock [15,16], and concrete structures [17,18], because AE is well suited for homogeneous or qusai-homogeneous materials with good acoustic transmission. However, its application to heterogeneous materials such as masonry is much more problematic [19].

*Correspondence to: Jie Xu, School of Civil Engineering/Key Laboratory of Coast Civil Structure Safety, Ministry of Education, Tianjin University, Tianjin 300072, China.
†E-mail: jxu@tju.edu.cn

The application of AE monitoring to masonry structures is highly complicated, as attenuation and wave propagation are dependent on the heterogeneity of the material. Besides, the presence of voids, cracks, and cavities does also influence the AE detection itself. The AE waves, generated at the other side of a large crack to which the sensors are placed, will generally not be detected by AE sensors. This, for example, would be the case between the disconnected layers of a multiple-leaf wall, which is often encountered in historical masonry structures. All these ingredients make the source localization in masonry structures rather difficult [7]. Attempts were made in [20], involving the location of cracks during an on-site monitoring campaign. Although a large amount of AE events were detected, only a small percentage of them could be located. Damage location in masonry arch bridges was performed in [21] by simply applying a large set of AE sensors and identifying the sensors where most damage was detected. Some soft computing methods, such as optimized sensor triangulation procedure [22], smart sensor technology [23], neural-network approach [24], and multiway partial least square method [25] were employed into the damage detection of composite material in aircraft. Because of the reasonable detection results from these application, these methods may also can be introduced into the masonry damage detection application. But much more research should be performed if we want to transfer one technique from one field to another because the composite material in civil engineering is totally different with that in the aircraft.

This paper focuses on the applicability of AE technique in order to assess damage regions in masonry structures. An improved approach, modified from the classical crack source localization method, is proposed to provide more reliable crack locations in masonry structures. A series of tests were designed and carried out on a masonry bridge model, and the results of the tests are discussed in the following text.

## 2. SOURCE LOCATION OF AE EVENTS

Localization of AE sources is important to assess the regions of active damage in the monitoring technique. Location problems are usually solved by various triangulation techniques based on mathematical analysis of acoustic wave trajectories [26,27]. This analysis cannot be simply performed if the structure of tested specimen is geometrically complicated. Generally, these techniques depend on the mode of propagation, the elasticity modulus, and signal attenuation due to the heterogeneity and anisotropy of material. In this section, a general overview on the classical localization method and the corresponding knowledge is depicted.

### *2.1. Onset time determination of the acoustic signals*

Source localization is based on the onset times or arrival times of the direct body waves. Theoretically, onset times of the direct body waves, *P*-wave and *S*-wave, both can be used for source localization. However, only first wave onset times (*P*-times) are usually measurable, because multiple side reflections, structural noise, and sensor response will interfere the later phases.

The true onset time of a crack AE event could be described as the moment when the first energy of a particular signal phase reaches the sensor positions [28]. In signal analysis, the onset time is usually picked as the point where the first difference between the signal and the noise takes place [29]. Determination of the onset time of AE signals is crucial for the whole localization process and is the major premise to affect the localization accuracy [8].

Manually picking is the preferred choice if there are only few events available. It is still necessary to have reliable automatic picking tools, because human analysts cannot manage the vast amount of data recorded in the monitoring. In concrete monitoring, many algorithms have been proposed for automatic detection of onset times. Two mostly used methods, short term average/long term average (STA/LTA) picker by [30] and AIC-picker [31] are employed and investigated for the AE signals in masonry structures. The picking accuracy of the STA/LTA-picker and AIC-picker was quantified by a comparison with picks that were set manually.

For 1122 signals of AE events recorded at the pencil-lead break tests in Sections 3 and 4, the differences $\Delta t$ between the automatic and the manual picks are examined. Figure 1 shows the results for the STA/LTA-picker and for the AIC-picker, compared with manually picked onset times.



DOI: 10.1002/stc

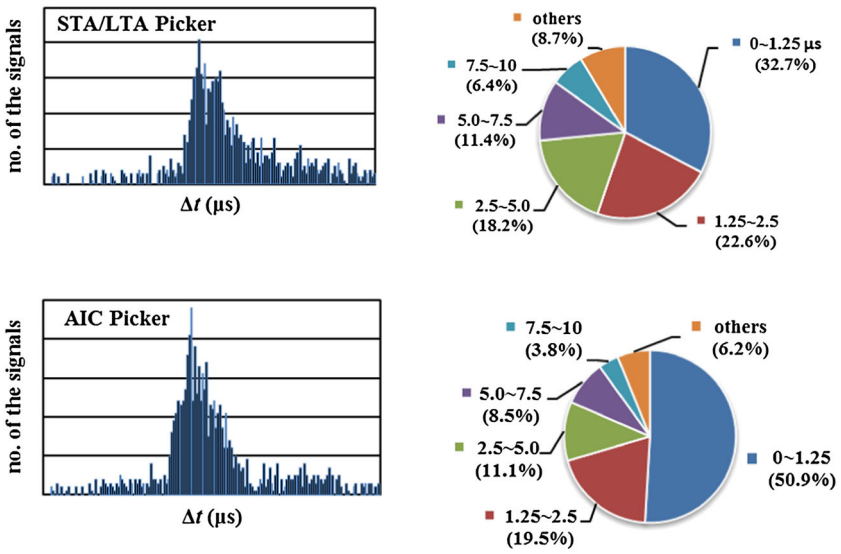


Figure 1. Differences $\Delta t$ between automatically and manually picked arrival times for the short term average/long term average (top) and the AIC-picker (bottom). The pie charts show the performance of both automatic pickers.

The signals have different reading precisions of their first onsets, depending on the signal-to-noise ratio and how impulsive onsets are. The results from the two methods are both acceptable, although the STA/LTA-picker obviously shows a trade-off. With the AIC-picker, almost twice as many signals than the STA/LTA-picker are picked in a very good correlation, $\Delta t \leqslant 1.25$ μs. Also, the number of mispicks with $\Delta t \geqslant 5$ μs in the noise and picks too late in the signal could be reduced from 26.5% of that in STA/LTA-picker to 18.5%. Accordingly, the AIC-picker can be suggested as a reliable and accurate algorithm to determine the onset times of AE signals in masonry structures.

### 2.2. *Classical localization method*

As shown in Figure 2, in a theoretical model with wave propagation velocity $v_{Pi}$, the onset time $t_i^*$ at sensor $\overrightarrow{x_i}$, unknown crack coordinates $\overrightarrow{x_0}$, and origin time $t_0$ can be estimated by an integral along the actual ray path $\Gamma_i$:

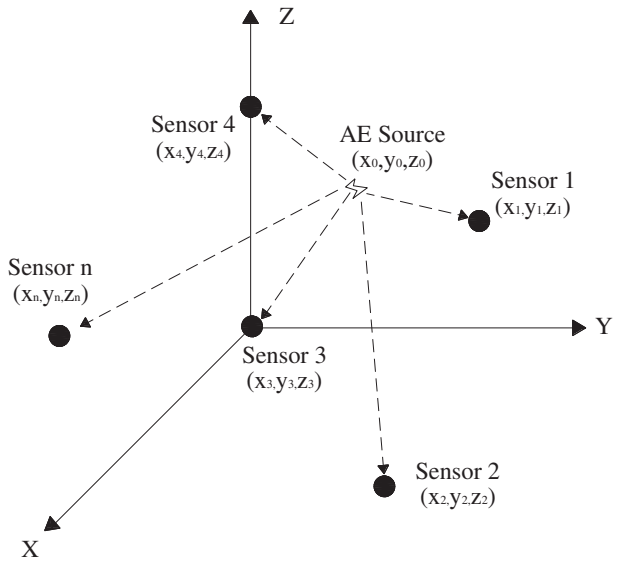


Figure 2. Localization of point acoustic emission source involving a generic array of $n$ sensors.



DOI: 10.1002/stc

$$t_i^* = t_0 + \underbrace{\int_{\Gamma_i} \left(d\Gamma_i / v_{Pi}(\mathrm{r})\right)}_{I}, \tag{1}$$

where $v_{Pi}(\mathrm{r})$ is the wave velocity field in the specimen or structure. If the material is homogeneous, Equation (1) can be simplified as

$$t_i^* = t_0 + \frac{\left|\overrightarrow{x_0} - \overrightarrow{x_i}\right|}{v_p} = t_0 + \frac{\overrightarrow{x_{i0}}}{v_p}. \tag{2}$$

For each sensor $i$, there will be residual $r_i$ between the detected onset time $t_i$ and the calculated onset time $t_i^*$:

$$r_i = t_i - t_i^*. \tag{3}$$

If $t_j$ is the onset time at another sensor $\overrightarrow{x_j}$, the measured onset time difference between sensors $i$ and $j$ is used. Usually, we have

$$r_{ij}{}^* = \Delta t_{ij} - \frac{\left(\overrightarrow{x_{i0}} - \overrightarrow{x_{j0}}\right)}{v_p}, \quad (i \neq j). \tag{4}$$

Usually, one sensor is taken as a reference sensor, which can be arbitrarily chosen, for example, assigned the sensor $j = 1$ as the reference sensor. Then, Equation (4) is

$$r_i{}^* = \Delta t_{i1} - \frac{\left(\overrightarrow{x_{i0}} - \overrightarrow{x_{10}}\right)}{v_p}, \quad (i = 2, \ldots, n) \tag{5}$$

If there are more than four onset times available for one event, the problem is overdetermined. These residuals are minimized using the least square method, in which the total error for $(n-1)$ Equations is simply the sum of all squared time-residuals:

$$\chi^2 = \sum_{i=2}^{n} \left(r_i^*\right)^2. \tag{6}$$

Residuals are reduced by applying corrections $\Delta \rightarrow x$ and $\Delta v_p$ to the source parameters, which can be written as

$$A^T A \overrightarrow{r} = -\mathrm{A}\left(\Delta \overrightarrow{x},\ \Delta v_p\right)^T. \tag{7}$$

Thereby, $\overrightarrow{r}$ is the data vector with the residuals for $n$ observations of an event. **A**, which is a $(n-1) \times 4$-matrix, contains the partial derivatives of the calculated travel times with respect to the source coordinates, calculated at $\overrightarrow{x_0}$:

$$A = \begin{pmatrix} \frac{\partial r_2^*}{\partial x} & \frac{\partial r_2^*}{\partial y} & \frac{\partial r_2^*}{\partial z} & \frac{\partial r_2^*}{\partial v_p} \\ \vdots & \vdots & \vdots & \vdots \\ \frac{\partial r_n^*}{\partial x} & \frac{\partial r_n^*}{\partial y} & \frac{\partial r_n^*}{\partial z} & \frac{\partial r_n^*}{\partial v_p} \end{pmatrix}_{\overrightarrow{x_0}}. \tag{8}$$

Due to the linearization of Equation (7), the problem is solved iteratively until convergence, starting with an initial guess for the crack source location.

### *2.3. Initial guess selection*

As described in Section 2.2, in order to solve the Equation (7), an initial guess to start the iteration calculation is necessary. From a mathematic point of view, a good initial guess is important to reduce the iterative steps and to increase the accuracy of the final result. In AE applications, however, methods to give the initial guess are rarely mentioned in existing publications. If an arbitrary value based on the subjective opinion of operator is chosen as the initial guess, the calculation will be time-consuming because of the greater iterative steps and the result may be unacceptable. Accordingly, a general method is proposed in this section to give a reliable and logical initial guess.



DOI: 10.1002/stc

The method is based on the Equation (2), in which the material is homogeneous. If the medium of interest is homogeneous and isotropic, wave propagation velocity $v_p$ is determined independently from AE measurement and the propagation direction, but only related to Lame constants $\lambda$ and $\mu$, and density $\rho$:

$$v_p = \sqrt{\frac{\lambda + 2\mu}{\rho}}. \tag{9}$$

Considering the unknown crack source $\overrightarrow{x_0}$ and the sensor $\overrightarrow{x_i}$ (Figure 2), the distance $\overrightarrow{x_{i0}}$ is

$$d_i = \left[(x_0 - x_i)^2 + (y_0 - y_i)^2 + (z_0 - z_i)^2\right]^{1/2}. \tag{10}$$

If we take the sensor $\overrightarrow{x_1}$ as the reference one, we have the Equations for the sensors $\overrightarrow{x_i}$ and $\overrightarrow{x_j}$:

$$\begin{cases} \overrightarrow{x_{i0}} - \overrightarrow{x_{10}} = v_p(t_i - t_1) \\ \overrightarrow{x_{j0}} - \overrightarrow{x_{10}} = v_p(t_j - t_1) \end{cases} \quad (i \neq j \neq 1). \tag{11}$$

Through mathematical manipulation, we have

$$[A\ B\ C]\begin{Bmatrix} x_0 \\ y_0 \\ z_0 \end{Bmatrix} = [E] \tag{12}$$

where

$$\begin{aligned} A &= 2\left[\Delta t_{j1}(x_1 - x_i) - \Delta t_{i1}(x_1 - x_j)\right] \\ B &= 2\left[\Delta t_{j1}(y_1 - y_i) - \Delta t_{i1}(y_1 - y_j)\right] \\ C &= 2\left[\Delta t_{j1}(z_1 - z_i) - \Delta t_{i1}(z_1 - z_j)\right] \\ E &= \Delta t_{i1}\left[\left(x_j^2 - x_1^2\right) + \left(y_j^2 - y_1^2\right) + \left(z_j^2 - z_1^2\right)\right] \\ &\quad - \Delta t_{j1}\left[\left(x_i^2 - x_1^2\right) + \left(y_i^2 - y_1^2\right) + \left(z_i^2 - z_1^2\right)\right] \\ &\quad + v_p{}^2\left(\Delta t_{j1}\Delta t_{i1}{}^2 - \Delta t_{i1} v_p \Delta t_{j1}{}^2\right) \end{aligned} . \tag{13}$$

In Equation (13), all the variables are either known or can be measured, thus if the onset times are available and together with the predetermined velocity $v_p$ by Equation (9), three linear independent Equations can be formed in this manner and unknowns $(x_0, y_0, z_0)$ in Equation (12) can be solved.

Thus, $(x_0, y_0, z_0, v_p)$ can be used as the initial guess value to start the iterative calculation. Obviously, if the material is strictly homogeneous, our initial guess is exactly the final required result. Therefore, the initial guess from the proposed method is sure to give a more reliable and logical result than the arbitrary chosen values.

### *2.4. The AE velocity field $v_{Pi}$(r)*

As shown in Equation (1), the wave velocity field $v_{Pi}$(r) is an important factor in the calculation. The variation of $v_{Pi}$(r) is affected essentially by the material property of tested structures. If the structure can be considered as homogeneous, the wave path from the crack source to the sensor is certainly considered to be a straight line, shown by dashed straight line in Figure 2 and the $v_{Pi}$(r) is also homogeneous. In this case, the velocity inside the structure is a unique value in each path direction and the value $v_P$ can be estimated by Equation (9). The metal is the typical material that can be considered as homogeneous, in which the Equation (2) can be applied well [32].

The concrete cannot be thought to be homogeneous if compared with the metal structure, whereas the Equation (2) under the homogeneous assumption is still applicable. For concrete, this assumption is reasonable, because for waves with a wavelength of, for example, $\lambda \approx 20$ mm (for a frequency $f = 200$ kHz and $v_p = 4000$ m/s [33]) signal aggregates or pores are not resolved, though these inhomogeneities have a great influence on the propagating wave field. The propagation speed can be averaged over the propagation path. The ray path $\Gamma_i$ can be treated approximately the same as calculated distance $ds$



DOI: 10.1002/stc

between the sensor and the crack source, shown in Figure 3(a). The validation of this assumption has already been testified by numerical analysis of the 2D modeling [11]. One of the main difficulties is the strong scattering of the waves at those aggregates having a characteristic length similar to the wavelengths.

However, for the masonry structures, the reflection and refraction of the wave at the layers is unavoidable. Here, we only consider the propagation effects related to the refraction of AE wave, because the reflection mostly ascribes to the decreasing of the incident power density and of the signal amplitude. From Figure 3(b), the propagation delays (denoted as *P*-D) are

$$P\text{-}D = \frac{\Gamma_i}{v_\Gamma} - \frac{ds}{v_{ds}} = \frac{\int_{\Gamma_i} k\, dl}{v_{ds}} - \frac{ds}{v_{ds}}, \tag{14}$$

where $k = \frac{v_{ds}}{v_\Gamma}$ and $v_\Gamma$ is the wave propagation velocity along the ray path $\Gamma$ and $v_{ds}$ is the counterpart along the calculated path *ds*. Then, we have

$$P\text{-}D = \underbrace{\frac{\int_{\Gamma_i} kdl}{v_{ds}} - \frac{\int_{\Gamma_i} dl}{v_{ds}}}_{\text{Velocity } \textit{delay}} + \underbrace{\frac{\int_{\Gamma_i} dl}{v_{ds}} - \frac{ds}{v_{ds}}}_{\textit{Geometrical}\text{ delay}}. \tag{15}$$

Usually, the velocity difference in the two paths for one sensor event is not very significant and $k = 1.0$. Therefore, only the propagation effect of the geometrical delay is considered,

$$P\text{-}D = \frac{\int_{\Gamma_i} dl}{v_{ds}} - \frac{ds}{v_{ds}}. \tag{16}$$

In general, the *P-D* value reflects deviation of the real wave propagation path $\Gamma_i$ from the calculated path *ds* between the sensor and the crack source. The value will increase as the distance increases, because the conditions are more complicated for traveling through more layers. In this respect, the *P-D* is unavoidable, existing in the masonry structures, which means the classical method based on Equation (2) cannot be used directly here.

## 3. EXPERIMENTAL SETUP AND OPERATION

According to the aforementioned crack source localization problem in masonry structure, several tests based on a two-arch masonry model bridge are operated in this research.

### *3.1. The model bridge*

A two-arch masonry model bridge (Figure 4), designed according to historical rules for the geometry definition and sharing most of the characteristics of real historical bridges, is investigated. According to

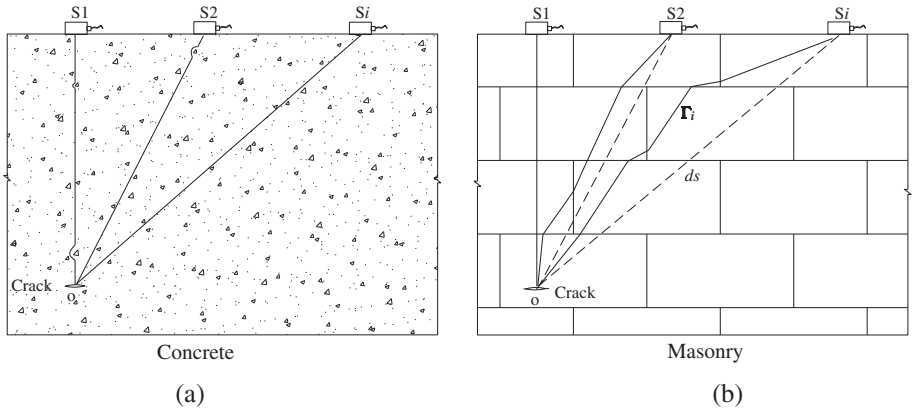


Figure 3. Schematic descriptions of the differences between real wave propagation path and the theoretical path in concrete (a) and masonry (b).



DOI: 10.1002/stc


Figure 4. Model bridge realized at the Politecnico di Torino laboratory.

the theory of models, the geometry is scaled down to obtain the model dimensions. The scale of the model bridge is 1 : 2 and it is 5.90 m length, 1.60 m width, and 1.75 m height. Constituent bricks made by hand have a uniform size of $130 \times 65 \times 30$ mm, according to the geometrical scale proportion. Strength and stiffness of masonry brick and mortar have been selected to better reproduce the case of real historical bridges.

The model bridge is supported by two masonry abutments and a central pier built with the same masonry. The abutments lay on concrete basements that are linked to the ground through special reinforcements.

Above the arches, there are containment masonry walls on the four sides of the bridge, which provide the location for the filling material. The upper part of the bridge is completed with a concrete slab top, realized with limited cement content.

### *3.2. Mechanical parameters for the model bridge*

Prior to the tests, it is useful to estimate the mechanical parameters of the bridge. The mechanical parameters to collect are those of the basic material, that is, the masonry.

A number of laboratory tests have been performed (Figure 5), including compression tests, diagonal compression tests, four-point bending tests on masonry arches, and shear tests. In addition, tests on the mortar alone, and on the concrete used to support the abutments have been performed. The main mechanical parameters obtained are the following: the Young's modulus $E$, the Poisson ratio $v$, the tensile strength $f_t$, the compressive strength $f_c$, and the tensile fracture energy $G_F$. The detail description of the tests can be found in [34], and the useful mechanical parameters for our research are listed in Table I.

### *3.3. Pencil-lead break tests*

In order to analyze the AE propagation property in masonry, it is necessary to know the actual AE source locations. Usually, artificial sources, such as Capillary break, small ball bearing drop, pulsed AE sensor, and pencil-lead break are commonly used for calibration purposes or to study wave propagation in solids. Probably the most used source as a simulated source of AE is the pencil-lead break test [35]. Therefore, pencil-lead break tests with artificial sources at defined positions on the masonry bridge are carried out, which has the similar procedure with that operated in concrete structures [8].

### *3.4. AE monitoring system*

An AE measurement system (ATEL device) consisting of six piezoelectric (PZT) sensors and six control units is used to record AE signals in our research, shown in Figure 6. The PZT sensors exploit the capacity of certain crystals to produce electric signals whenever they are subjected to a mechanical stress. The sensors are attached to the masonry surface, which is carefully smoothed by means of vacuum silica grease. The ATEL sensors, acting as strainmeters, transform mechanical vibrations (AE) of about $10 \pm 7$ mm amplitude into electrical signals (AE signals) of about $10 \pm 6$ V amplitude.



DOI: 10.1002/stc

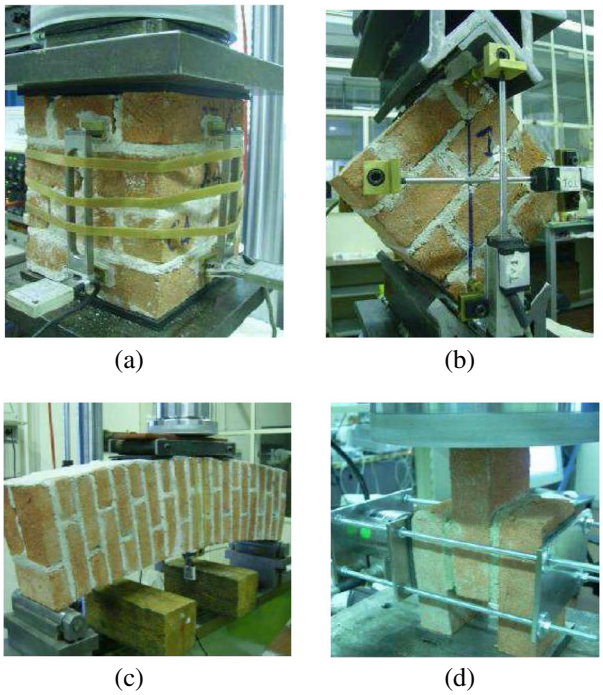

(a) (b)

(c) (d)

Figure 5. Laboratory tests for the mechanical characterization of the masonry: (a) compression test; (b) diagonal compression test; (c) four point bending of a masonry arch; and (d) shear test.

Table I. Mechanical materials parameters obtained from the tests.

| Parameter | $\gamma$ [kg/m$^3$] | $E$ [Pa] | $v$ | $f_c$ [Pa] | $f_t$ [Pa] | $G_F$ [Nm] |
|---|---|---|---|---|---|---|
| value | 1900 | $1.5\times10^9$ | 0.2 | $3\times10^5$ | $4.3\times10^6$ | 400 |

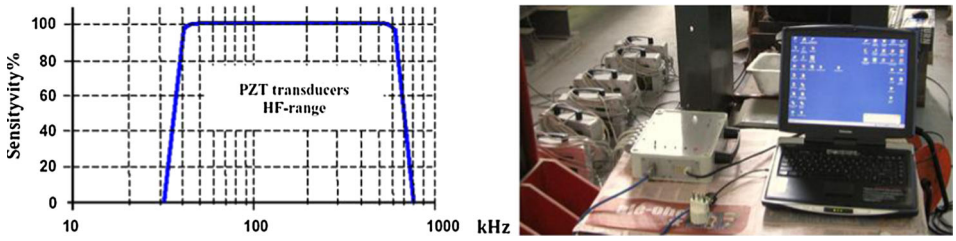


(a) (b)

Figure 6. (a) Frequency bands of sensitivity for the acoustic emission (AE) sensors used in the acquisition; (b) control units and acquisition system used to record AE signals.

In the graph shown in Figure 6, the maximum sensitivity of PZT transducer is displayed. The PZT sensors have a linear frequency response of between 50 and 500 kHz. Considering unknown a priori the amplitude levels in the HF-range, the AE transducer has been selected on the basis of its great sensitivity and with a threshold voltage $A_{th}$ (here, fixed at 100 μV in order to filter out the environmental noise).

They are connected to preamplifiers and then to the acquisition unit. Signal detection is triggered dependently for each channel by a fixed threshold. With the help of the software Labview, transient signals with 10 MHz sampling rate are recorded for later extraction of the first onsets and source localization.



DOI: 10.1002/stc

### *3.5. AE signal Attenuation test*

A series of pencil-lead break tests are performed on the central pier of the bridge to study the attenuation and the velocity properties. The size of the central pier is of 160 × 50 × 28 cm, shown in Figure 4, and it can be considered as a representative masonry solid structure.

The released energy is an important source parameter for an AE event. With every crack, energy is released within the material and a transient elastic wave is generated. The effectiveness of the AE technique for masonry is primarily reliant on the acoustic transmission of the mortar joints and on the quality of the mortar and masonry units. In order to define the applicability of AE for locating cracks and crack propagation, attenuation of AE signals need to be considered.

Pencil-lead break tests are performed on the pier at increasing distances to analyze the wave attenuation when propagating in both surface (shown in Figure 7) and body conditions. Signal shape is stored, and the energy is measured following transmission through the mortar joints in the latitudinal direction (9.5-mm-thick joints at 130 mm distances); see Figure 7. One sensor is used to detect AE signals from sources at increasing distances of 10 cm on the surface, in which the pencil-lead break point and the sensor are in the same surface of the central pier. The process is carried out for the central pier as well as for the concrete basement (shown in Figure 4a) on the surface for comparative purposes. For the masonry, the body condition, in which the break point is on one surface and the sensor is on the other side surface of the middle pier to simulate the wave propagation inside of the body, is also investigated. The total energy $W$ released by an AE event is defined in this study as the total value of area under the acoustic signal in the signal duration. The attenuation result is shown in Figure 8.

From Figure 8, the AE signal transmission loss in masonry is much higher than in concrete because of the numerous boundaries between the bricks and mortar joints in the masonry. There is, for example, approximately 22% reduction in energy when measured at a surface distance of 60 cm from the AE source in concrete, but 45% of the total energy is lost in masonry. If the wave propagates inside the masonry pier, only 16% of the total energy remains. When the distance is further than 80 cm, it is

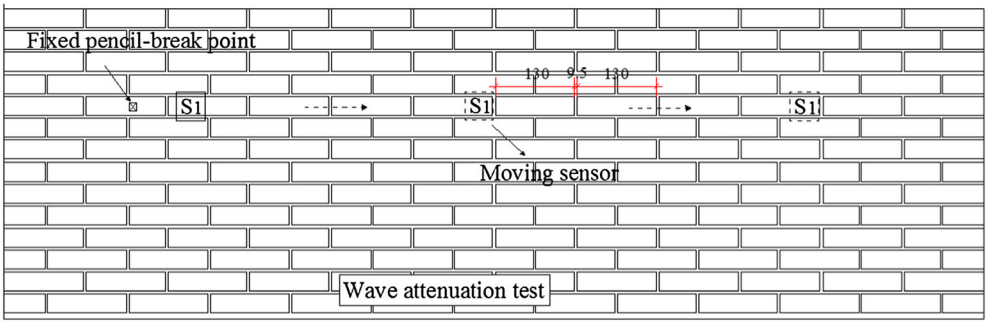


Figure 7. The sketch of fixed pencil-lead break point and the moving sensor in the attenuation test on the central pier.

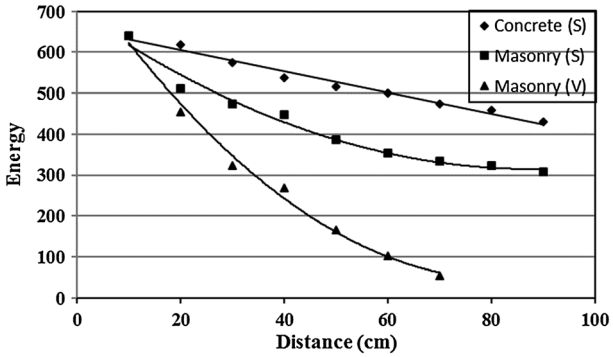


Figure 8. Conditions of acoustic emission signal attenuation in concrete and masonry.



DOI: 10.1002/stc

difficult to record the signals through the body, because the signal is almost attenuated or mixed in the noise, which is almost no use for our analysis. Here, we recommend the signal to be discarded when its percentage of energy remaining is below 15% of the total energy. In order to locate the cracks within the structure it is determined that the sensors needed to be placed no more than 60 cm apart in the body and 100 cm on the surface. Of course, this distance depends on the layout of the bricks, the quality of the mortar-brick connection and the coherence of the masonry in general.

### *3.6. Wave velocity tests*

Six sensors ($S_0$–$S_5$) are used to detect AE signals, and the distance between two adjacent sensors increased from $S_{1-0}$ to $S_{5-4}$ with an increment of five units, shown in Figure 9. On one hand, the pencil is broken beneath the sensor $S_0$ with 5-cm distance away in the same surface to study the surface velocity propagation, which is the scenario shown in Figure 9. On the other hand, wave propagation inside masonry body condition is also investigated by using the same sensors at the same positions and breaking the pencil at the same corresponding position of the sensor $S_0$, but on the opposite surface of the central pier.

The results of the measured velocities are shown in Figures 10 and 11. The velocity named V-homogeneous, is calculated according to Equation (9) based on the mechanical parameters in Table I for comparison purpose. The V-average is the average velocity value of all the calculated velocities in the corresponding test.

In Figures 10 and 11, the velocities, detected both on the surface and inside of the masonry, clearly show that the value of the velocity decreases with the increasing traveling distance. The reason for this is that the transient wave changes its mode many times from longitudinal to shear and/or to surface waves and vice versa due to the reflection and/or refraction during traveling in different phases. The


Figure 9. Wave velocity test: (left) the sketch of the pencil-lead break point and the sensor distribution; (right) scenario of the velocity test.

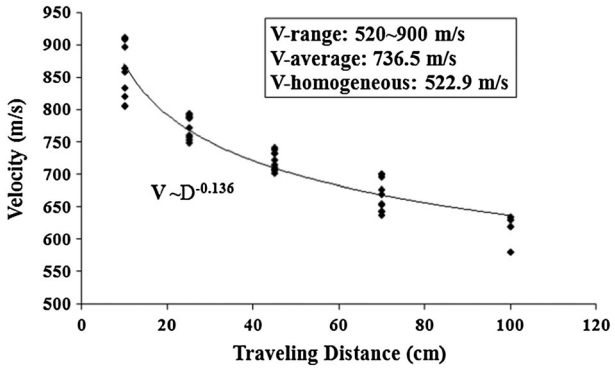


Figure 10. Wave velocity of the acoustic emission on the surface of masonry model bridge.



DOI: 10.1002/stc

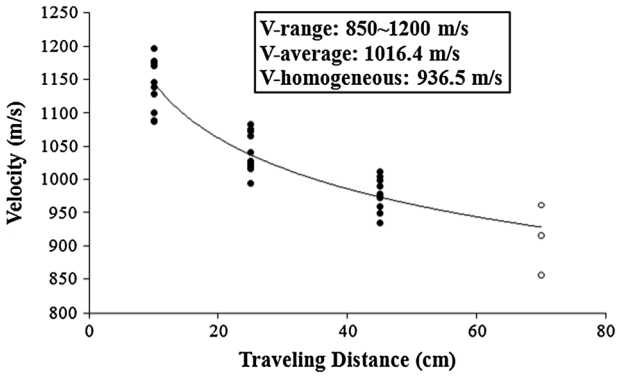


Figure 11. Wave velocity of the acoustic emission inside masonry bridge. The empty circles means the results are not so accurate because of the bad signal quality.

longer the traveling distance, the more change happens, which leads to a greater deviation of the real wave propagation path $\Gamma_i$ from the calculated path *ds*. This is what we called propagation delay phenomenon in Equation (14).

Another issue noted in the Figures 10 and 11 is that the V-homogeneous has a great difference with the V-average, which means we cannot use the velocity value from Equation (9) by taking the masonry as a homogeneous material in initial guess. Thus, the V-average from the velocity test is adopted as the velocity value in the initial guess to start the iteration of source localization calculation.

## 4. THE AE SOURCE LOCALIZATION IN MASONRY

### *4.1. The modified crack source localization method*

The classical localization method can be used in the concrete structures according to the analysis in Section 2.4. But the localization of AE source in masonry structures is highly complicated, as attenuation and wave velocity are dependent on the heterogeneity of the material (not only the interface between bricks and mortar, but also cracks and cavities in existing structures). The theoretical analysis in Section 2.4 and the test result in Section 3.6 both illustrate that the classical localization method based on Equation (2) cannot be used directly in masonry. A modified method based on the classical method is introduced in the following part.

The basic idea of the localization in masonry is the same as that in concrete. But propagation delay due to the layers in the masonry structures makes the homogeneous assumption is unavailable here. Modifications for propagation delay are implemented.

The geometry distance *ds* is still taken as the calculated path, because the detailed knowledge of the actual wave path $\Gamma$, is not possible to be known. But modification can be made for the time-delay according to the velocity property in Figures 10 and 11 to reduce the effect of inhomogeneous property. In the modified model, the classical model result in Equation (6) is modified into

$$\chi^2 = \sum_{i=2}^{n} {r_{i1}}^2 = \sum_{i=2}^{n} \left[\overrightarrow{x_{10}} - \overrightarrow{x_{i0}} - (k_i t_i - t_1)v_1\right]^2, \tag{17}$$

where $k_i = (d_1/d_i)^{\xi}$ is the modified factor, which is used to modify the effects of the inhomogeneity or propagation delay. The parameter $\xi$, denoted as degree of the inhomogeneity, in $k_i$ reflects the inhomogeneous degree of the material. The degree of the inhomogeneity $\xi$ is determined from the result of the pencil-lead break wave velocity test, shown in Figure 10. It reflects the relationship between the calculated velocity and the wave propagation distance. In strictly homogeneous materials, the value $\xi$ is 0 because the wave velocity is a constant value and does not changes with traveling distance. If the material is not homogeneous, value $\xi$ will theoretically increases with the degree of the heterogeneity. The degree of the inhomogeneity $\xi$ in our research is 0.14, which is taken from the relation between the velocity and traveling distance shown in Figure 10.



DOI: 10.1002/stc

For the initial guess selection, considering the complicated condition in masonry, localized result ($x_c$, $y_c$, $z_c$, $v_c$) from the classical method is taken as the initial guess for the modified model.

### *4.2. The procedure of the modified localization method*

Figure 12 shows that the procedure to determine the crack source by the modified localization method, obtained after the discussion from Section 2.1 to Section 4.1.

### *4.3. Comparison of the two methods*

*Ad hoc* tests are performed to reproduce AE source using pencil-lead break on the right-side surface of the masonry abutment. Six sensors introduced in Section 3.4 are attached to the surfaces, shown in Figure 13. In particular, 19 different pencil-lead break points (artificial source) are drawn on this surface, and for each point, the tip of a pencil is broken eight times, so a total of 152 measurements are recorded. For this test 912 AE events from the six sensors are obtained and then the source localizations of all the 19 points were calculated according to the procedure that expressed in Figure 12.

The results of the locations are shown in Figure 13 for both the modified and classical methods. It can be noted that the location accuracy varies with the position of the breaks. The break points can be approximately divided into three groups. The points 3–8 inside the central area of the sensor covered region (the dashed line in Figure 13) have the best crack source monitoring result for both classical and the modified methods. In the second group, including points 2, 9, 10, 11, and 12, points are distributed on the nearby region of the sensor covered region. The rest of the points, far from the sensor covered region, are in the third group.

For points in the first group, both methods give the ideal result, all the errors are smaller than 6 mm, and most of the crack events can be monitored. For the second group, the modified model shows better results than the classical method. The errors (*a* value in Figure 13) in the classical method are about 15–75 mm, whereas the counterparts (*b* value in Figure 13) can be reduced to about 6–27 mm in the modified method. In this condition, about half of the break events can be detected according to the *c* value in Figure 13. The result from the classical method for the third group is barely acceptable for its exaggerated errors, whereas modified method is still in good conditions. Although the errors were slightly large, about three or four centimeters, the results are still acceptable considering the entire size scale of the surface.

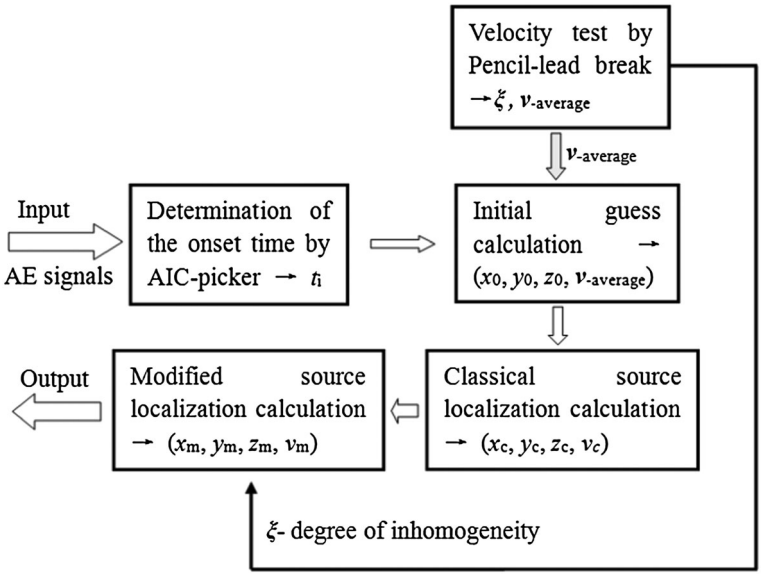


Figure 12. Flow-chart of the modified crack source localization method to determine the acoustic emission source locations.



DOI: 10.1002/stc

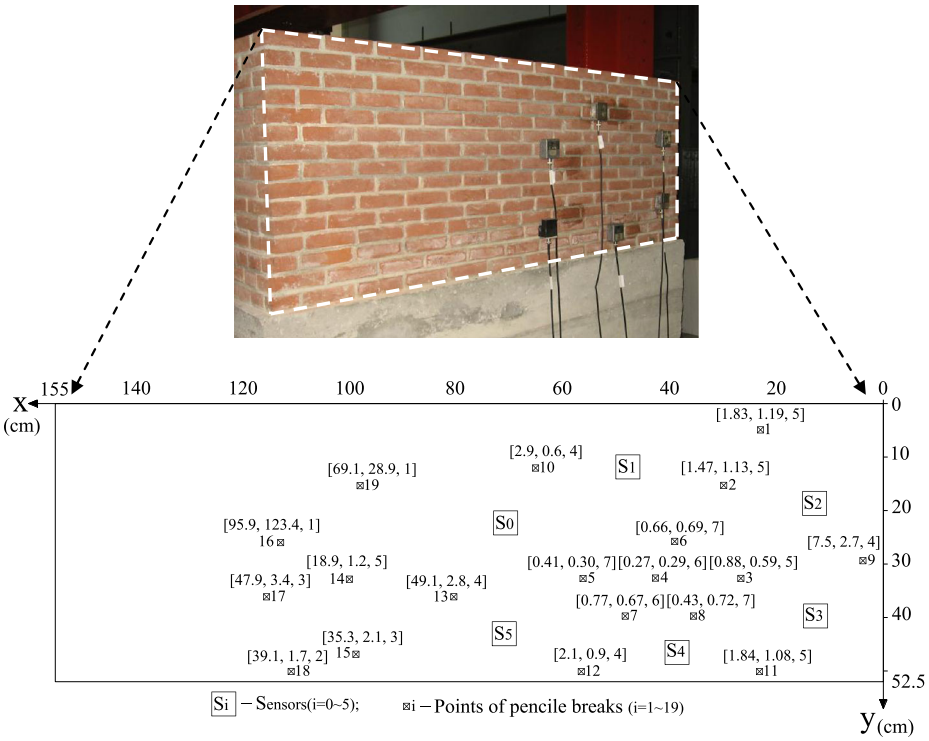


Figure 13. Results of the source localization calculated from the classical and the modified methods. In [*a*, *b*, *c*], *a* is the average error of all the available breaks from the classical method, and *b* is the average error of all the available breaks from the modified method, and *c* is the available breaks that can be used for each point.

Three representative points, 4, 10, and 17, respectively, of the three groups are selected to give the detailed results in Figure 14.

From the results in Figures 13 and 14, the importance of sensor arrangement for the localization capability can also be noted. For a given sensor distribution and an arbitrary AE source position, the localization accuracy can be quantified. The highest accuracy can be achieved for events inside the volume spanned by the sensors, such as points of the first group. Distances of sources far from the sensor network are less accurate or of little use. These conclusions can help to emphasize the importance of the sensor arrangement and to remind us to select proper attached positions for AE sensors instead of randomly distributions.

Altogether, the three conditions show that in comparison with the classical method, the modified method appears to give excellent results for the masonry structure in the source localizations.

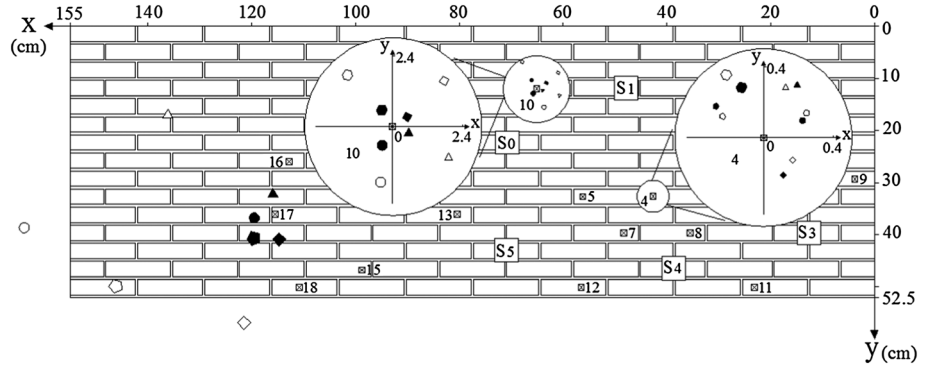


Figure 14. Detailed localization results of the point 4, point 10, and point 17. The solid points represent the results of the modified method and the empty points of the classical method.



DOI: 10.1002/stc

Figure 15. The monitored conjunction before the test (left); the comparison of the crack positions between the experiment and the acoustic emission monitoring. The black points are the results from the modified model (right).

### *4.4. Central pier settlement test*

Experiment of applying different settlements on the central pier to simulate the damage of scour are operated on the masonry model bridge. Differential settlement with an upper bound of 20 mm was applied incrementally to the central pier, and the detail description of the experiment can be found in [34]. During the settlement test, AE technique is employed to monitoring the crack location by our proposed modified method.

Four sensors were arranged around the pier-arch conjunctions according to the analysis before the test, and the AE monitoring system was the same as that used in the pencil-break test. The monitoring results are shown in Figure 15.

As for the AE monitoring, a total number of 23 AE points was localized by means of the modified method. Most of the localized points have a good agreement with the crack pattern configuration by surrounding the main crack on the left conjunction between the pier and the arch.

## 5. DISCUSSION AND CONCLUSIONS

Monitoring techniques have received considerable attention due to the increasing demand of structural retrofit and strengthening. As one of the non-destructive monitoring techniques, acoustic emission is employed for the masonry cracking analysis.

For AE applications in monitoring, localization of AE sources is important to offer the information of the active damage region. The investigation of the localization accuracy has shown that monitoring results are greatly influenced by the structure material. The traditional localization method is mostly adopted to realize the localization in metal and concrete structures. However, for the masonry structures, the complicated material properties make the classical localization method not directly applicable.

The modified localization method proposed in this paper allows giving reasonable location results. In the modified method, a modified factor $k_i$ related to inhomogeneous or propagation delay is introduced. The degree of the heterogeneity $\xi$ in $k_i$ plays a key role to eliminate the effect of the inhomogeneous of the material. Accordingly, the pencil-lead break velocity tests on the masonry structure to measure the relation between wave velocity and traveling distance should be fulfilled before the monitoring. Based on this test result, the value $\xi$ can be obtained and employed in the monitoring process.

The sensor arrangement is another task that should be carefully considered. The investigation of the localization accuracy has shown that the sensor distribution is essential for monitoring AE activity in the specimen. The ideal condition is to ensure that all relevant regions are covered by enough sensors before the monitoring starts. Events detected are only a fractional amount of all recorded AE signals and, again, only a limited number of all detected events can be localized with a sufficient accuracy. For a good imaging of crack progression, it is necessary that enough events could be localized. Therefore, the proper arrangement of the sensors can give us more available points, which is well testified by the $c$ value in Figure 13.



DOI: 10.1002/stc

The results of an *ad hoc* experiment have shown that the results by the modified localization method are all located near the actual positions. This evidence allows considering the proposed method to be a reliable and suitable one compared with the classical method. In addition, the application of the modified method in the central pier settlement test confirmed the validity of the method. Thus, with the assistance of the reliable onset time picker (AIC-picker) and proper sensor distribution, the source localization in masonry can be realized properly by the modified model.

## ACKNOWLEDGEMENTS

The authors also thank Dr Manuello and Dr Niccolini for their help in the test and appreciate their suggestions. This research project is supported by the National Natural Science Foundation of China (No. 51178307) and Tianjin Natural Science Foundation (11JCZDJC24000). Support from the funding agency earlier is gratefully acknowledged.

## REFERENCES

1. Carpinteri A, Lacidogna G, Niccolini G. Acoustic emission monitoring of medieval towers considered as sensitive earthquake receptors. *Natural Hazards and Earth System Sciences* 2007; **7**:251–261.
2. Melbourne C, Tomor AK. Application of acoustic emission for masonry arch bridges. *Strain* 2006; **42**:165–172.
3. Carpinteri A, Invernizzi S, Lacidogna G. Structural assessment of a XVIIth century masonry vault with AE and numerical techniques. *International Journal of Architectural Heritage* 2007; **2**:214–226.
4. Carpinteri A, Lacidogna G. Damage monitoring of an historical masonry building by the acoustic emission technique. *Materials and Structures* 2006; **39**:161–167.
5. McCann DM, Forde MC. Review of NDT methods in the assessment of concrete and masonry structures. *NDT&E International* 2001; **34**:71–84.
6. Ohtsu M, Tomoda Y. Acoustic emission techniques for crack detection and damage evaluation. *Proc. of 1st Int. Rilem Symposium on Site Assessment of Concrete, Masonry and Timber Structures*, Binda L, Prisco Md, Felicetti R (eds). Varenna, Italy, 2008.
7. Verstrynge E, Schueremans L, Van Gemert D, Wevers M. Monitoring and predicting masonry's creep failure with the acoustic emission technique. *NDT & E International* 2009; **42**:518–523.
8. Carpinteri A, Xu J, Lacidogna G, Manuello A. Reliable onset time determination and source location of acoustic emissions in concrete structures. *Cement & Concrete Composites* 2012; **34**:529–537.
9. Chang PC, Flatau A, Liu SC. Review paper: health monitoring of civil infrastructure. *Structural Health Monitoring* 2003; **2**:257–267.
10. Grosse CU, Ohtsu M. *Acoustic Emission Testing: Basics for Research - Applications in Civil Engineering*. Springer: Berlin, 2009.
11. Schechinger B, Vogel T. Acoustic emission for monitoring a reinforced concrete beam subject to four-point-bending. *Construction and Building Materials* 2007; **21**:483–490.
12. Shiotani T, Aggelis DG, Makishima O. Global monitoring of large concrete structures using acoustic emission and ultrasonic techniques: case study. *Journal of Bridge Engineering* 2009; **14**:188–192.
13. Dutta D, Sohn H, Harries KA, Rizzo P. A nonlinear acoustic technique for crack detection in metallic structures. *Structural Health Monitoring* 2009; **8**:251–262.
14. Maslouhi A. Fatigue crack growth monitoring in aluminum using acoustic emission and acousto-ultrasonic methods. *Structural Control and Health Monitoring* 2011; **18**:790–806.
15. Eberhardt E, Stead D, Stimpson B. Quantifying progressive pre-peak brittle fracture damage in rock during uniaxial compression. *International Journal of Rock Mechanics and Mining Sciences* 1999; **36**:361–380.
16. Ganne P, Vervoort A, Wevers M. Quantification of pre-peak brittle damage: Correlation between acoustic emission and observed micro-fracturing. *International Journal of Rock Mechanics and Mining Sciences* 2007; **44**:720–729.
17. Carpinteri A, Lacidogna G, Niccolini G. Damage analysis of reinforced concrete buildings by the acoustic emission technique. *Structural Control and Health Monitoring* 2011; **18**:660–673.
18. Lovejoy SC. Acoustic emission testing of beams to simulate SHM of vintage reinforced concrete deck girder highway bridges. *Structural Health Monitoring* 2008; **7**:329–346.
19. Anzani A, Binda L, Mirabella RG. The effect of heavy persistent actions into the behaviour of ancient masonry. *Materials and Structures* 2000; **33**:251–261.
20. Carpinteri A, Lacidogna G, Manuello A, Binda L. Monitoring the structures of the ancient temple of Athena incorporated into the cathedral of Syracuse. *Proceedings of the 14th International Brick and Block Masonry Conference*, Sydney, Australia, 2008.
21. Carpinteri A, Lacidogna G, Invernizzi S, Manuello A, Binda L. Stability of the vertical bearing structures of the Syracuse Cathedral: experimental and numerical evaluation. *Materials and Structures* 2008; **42**:877–888.
22. LeClerc JR, Worden K, Staszewski WJ, Haywood J. Impact detection in an aircraft composite panel–a neural-network approach. *Journal of Sound and Vibration* 2007; **299**:672–682.
23. Coverley PT, Staszewski WJ. Impact damage location in composite structures using optimized sensor triangulation procedure. *Smart Materials and Structures* 2003; **12**:795–803.
24. Haywood J, Coverley PT, Staszewski WJ, Worden K. An automatic impact monitor for a composite panel employing smart sensor technology. *Smart Materials and Structures* 2005; **14**:265–271.
25. Mujica LE, Ruiz M, Berjaga X, Rodellar J. Multiway partial least square (MPLS) to estimate impact localization in structures. *7th IFAC Symposium on Fault Detection, Supervision and Safety of Technical Processes*. Barcelona, 2009.



DOI: 10.1002/stc

26. Ge M. Analysis of source location algorithms, part I: overview and non-iterative methods. *Journal of Acoustic Emission* 2003; **21**:14–28.
27. Ge M. Analysis of source location algorithms, part II: iterative methods. *Journal of Acoustic Emission* 2003; **21**:29–51.
28. Grosse CU, Finck F. Quantitative evaluation of fracture processes in concrete using signal-based acoustic emissions techniques. *Cement & Concrete Composites* 2006; **28**:330–336.
29. Kurz J, Grosse CU, Reinhardt HW. Strategies for reliable automatic onset time picking of acoustic emissions and of ultrasound signals in concrete. *Ultrasonics* 2005; **43**:538–546.
30. Baer M, Kradolfer U. An automatic phase picker for local and teleseismic events. *Bulletin of the Seismological Society of America* 1897; **77**:1437–1445.
31. Xu J. An effective way to validate signal arrival time in AE structural monitoring. *Advanced Materials Research* 2010; **163-167**:2471–2476.
32. Aljets D, Chong A, Wilcox S, Holford K. Acoustic emission source location in plate-like structures using a using a local triangular sensor array. *Mechanical Systems and Signal Processing* 2012; **30**:91–102.
33. Carpinteri A, Lacidogna G, Niccolini G. Critical behavior in concrete structures and damage localization by acoustic emission. *Key Engineering Materials* 2006; **312**:305–310.
34. Ruocci G. *Application of the SHM methodologies to the protection of masonry arch bridges from Scour*. Structural Engineering Department, Politecnico di Torino: Turin, 2009.
35. Scott IG. *Basic Acoustic Emission*. Gordon and Breach Science Publishers: Great Britain, 1991.



DOI: 10.1002/stc